Machine Copy for Proofreading, Vol. x, y–z, 2014

Sturm-Liouville Matrix Equation for the Study of Electromagnetic-waves Propagation in Layered Anisotropic Media

René Pernas-Salomón* and Rolando Pérez-Álvarez

Abstract—We obtain a Sturm-Lioville matrix equation of motion (SLME) for the study of electromagnetic wave propagation in layered anisotropic structures. Conducting media were taken into account so that ohmic loss is considered. This equation can be treated using a 4×4 associated transfer matrix ($\mathbf{T}$) in layered anisotropic structures, where the tensors: permittivity, permeability and the electric conductivity have a piecewise dependence on the coordinate perpendicular to the layered structure. We use the SLME eigenfunctions and eigenvalues to analyze qualitatively the numerical instability (Ωd problem) which potentially affects practical applications of the transfer matrix method. By means of the SLME coefficients we show analytically that $\mathbf{T}$ determinant value can be used to keep a check on the numerical accuracy of calculations. We derive equations to analyze wave propagation in linear layered isotropic structures. The SLME approach is applied on two typical layered structures to verify theoretical predictions and experimental results.

1. INTRODUCTION

A wide range of physical and technological problems can be described by equations of motion that follow the Sturm-Liouville matrix equation pattern (see, for example [1, 2] and [3], and citations therein). These problems includes many belonging to the elasticity theory (see for example [4]), electromagnetism [5] and other areas of classical physics. We can found SLMEs in Quantum Mechanics and Solid State Physics, particularly the Envelope Function Approximation (EFA) [6, 7] generates a massive class of equations of motion that follows the Sturm-Liouville equation in matrix form. Initially many of these equations of motion are three-dimensional, but in most of the heterostructures of interest which have planar geometry (two-dimensional (2D) slabs stacked along a growth direction — henceforth z-perpendicular to the planes of the interfaces, with 2D position vector $\overline{\rho} = (x, y)$) the problem can be reduced to a 1D problem. After 2D Fourier transform, which introduces a 2D wavevector $\overline{\kappa} = \kappa_1 \overline{e}_x + \kappa_2 \overline{e}_y$, the differential system is κ dependent and 1D in the variable z. In this way the equations of motion take the Sturm-Liouville form, namely [1]:

$$\frac{d}{dz}\left[\mathbf{B}(z)\cdot\frac{d\overline{F}(z)}{dz}+\mathbf{P}(z)\cdot\overline{F}(z)\right]+\mathbf{Y}(z)\cdot\frac{d\overline{F}(z)}{dz}+\mathbf{W}(z)\cdot\overline{F}(z)=\mathbf{0}. \tag{1}$$

This defines the matrix differential operator $\mathbf{L}(z)$. The unknown $\overline{F}(z)$ is a vector of N components, which can be: electronic wavefunctions, or envelope functions, if we deal with electronic states; vibration amplitude for elastic waves; or components of the electric field in some electrodynamic situations. The coefficients $\mathbf{B}(z)$, $\mathbf{P}(z)$, $\mathbf{Y}(z)$, and $\mathbf{W}(z)$ are square matrices of order N which describe properties of heterostructure constituting materials. The Equation (1) can be solved using two major mathematical tools: Green function techniques and the transfer matrix method [1].

In layered anisotropic structures the Maxwell's equations have been solved using different techniques. In his work, C. Oldano [8] used Maxwell's equations in Berreman's formalism [9] as starting

Received 5 November 2014

* Corresponding author: René Pernas-Salomón (rps@uaem.mx).
The authors are with Universidad Autónoma del Estado de Morelos, Ave. Universidad 1001, CP 62209, Cuernavaca, Morelos, México.

point to develops a 4×4 transfer matrix for nonabsorbing medium considering unit permeability. A method that combines Green-function and the transfer matrix techniques was developed in [10] for a first-order inhomogeneous differential equation obtained from Maxwell's equations in the presence of sources and unit permeability. A 4×4 transfer-matrix method to study the scatterings of electromagnetic waves by anisotropic metamaterials was established from classical Maxwell's equations in [11], but sources of EM field were not considered. In this work, we follow a different approach. In order to study a more general case, we used Ampère's law for a conducting medium to derive an Sturm-Lioville matrix equation (SLME) of motion for electromagnetic (EM) wave propagation in anisotropic layered media. This approach enable to cover a more real problem in which ohmic loss is considered.

From the formal point of view transfer matrix method (TMM) is suitable to study wave propagation in multilayer systems. However, in practical applications this method is hampered by numerical instabilities [12–15], the most common one being called the Ωd problem. The name associated to this numerical instability derives from the elastic waves studies where this instability arise at high frequencies ω and/or big thickness (d) of the layers. However, this numerical instability can potentially arise in any numerical application of the TMM where the matrix elements consist in the sum of real positive exponential terms and real negative exponential terms [1, 16]. If these sum becomes the sum of a very large number and a very small number (at high frequencies and/or big thickness of the layers, for example) the computer's rounding operations, which is one of the major sources of errors in numerical computations [17] lead to the Ωd problem. For the SLME the determinant of the associated transfer matrix $\mathbf{T}$ can be evaluated in terms of coefficients $\mathbf{B}(z)$, $\mathbf{P}(z)$, $\mathbf{Y}(z)$ [1] and we show that it could be a useful tool to control the numerical quality of calculations concerning EM wave propagation in layered media. This paper is organized in the following way: We first obtain an Sturm-Liouville matrix equation of motion for electromagnetic-waves propagation in Section 2 and introduce three important properties that support the use of this equation, in Section 2.1. We derive the corresponding equations and analyze wave propagation in linear layered isotropic structures in Section 3. In Section 4.1 we apply the SLME approach to a Fabry-Perot microcavity (a layered anisotropic system) and compare the results of our calculations with experimental results. In Section 4.2 we consider a porous silicon photonic mirror (a layered isotropic structure) to verify theoretical predictions and to illustrate numerical instability of matrix $\mathbf{T}$. Conclusions are presented in Section 5.

2. STURM-LIOUVILLE EQUATION OF MOTION FOR ELECTROMAGNETIC WAVES

Consider a linear layered anisotropic media. It means that we will work with constitutive relations: $\overline{D} = \hat{\epsilon}(\overline{r})\cdot\overline{E}$, $\overline{H} = \hat{\nu}(\overline{r})\cdot\overline{B}$ and $\overline{j} = \hat{\sigma}(\overline{r})\cdot\overline{E}$. Vectors $\overline{E}$ and $\overline{H}$ are the electric and magnetic field strength respectively, $\overline{D}$ is the electric displacement, $\overline{B}$ the magnetic flux density and $\overline{j}$ the electric current density vector. The permittivity tensor was denoted by $\hat{\epsilon}$ and $\hat{\nu}$ represent the inverse of permeability tensor $\hat{\mu}$. $\hat{\sigma}$ denotes the electric conductivity tensor.

We assume that heterostructures have planar geometry. Then the above space dependent tensors $\hat{\epsilon}$, $\hat{\nu}$ and $\hat{\sigma}$, which are symmetric, will depend on z coordinate only, and the components of $\overline{E}$, $\overline{B}$ and $\overline{H}$ can be expressed as:

$$E_m(\overline{r},t) = -\left(\frac{\partial\psi_0}{\partial x_m} + \frac{\partial\psi_m}{\partial t}\right) = E_m(z)e^{i(\kappa_1 x+\kappa_2 y-\omega t)}; \tag{2}$$

$$B_m(\overline{r},t) = \sum_j\sum_n e_{mjn}\frac{\partial\psi_n}{\partial x_j} = B_m(z)e^{i(\kappa_1 x+\kappa_2 y-\omega t)}; \tag{3}$$

$$H_m(\overline{r},t) = \sum_j\sum_s\sum_n \hat{\nu}_{mj}e_{jsn}\frac{\partial\psi_n}{\partial x_s} = H_m(z)e^{i(\kappa_1 x+\kappa_2 y-\omega t)}, \tag{4}$$

where

$$\psi_\eta = \psi_\eta(z)e^{i(\kappa_1 x+\kappa_2 y-\omega t)}; \quad \eta = 0,1,2,3. \tag{5}$$

Here ψ_0 denotes the scalar potential, $\overline{\psi} = (\psi_1,\psi_2,\psi_3)$ is the vector potential and ω is the frequency. Hereafter, subindexes (s, j, m, n) take values from 1 to 3 and coordinates x_1, x_2, x_3 represent x, y, z

coordinates respectively. We used a Levi-Cevita symbol e_{mjn} to express cross product in expressions (3) and (4).

The Ampère's law can be written in the form of scalar partial differential equations:

$$\sum_j \sum_m e_{njm} \frac{\partial H_m(\overline{r},t)}{\partial x_j} + i\omega \sum_m \tilde{\epsilon}_{nm} E_m(\overline{r},t) = 0; \quad n = 1,2,3, \tag{6}$$

where the tensor element $\tilde{\epsilon}_{nm} = \hat{\epsilon}_{nm} + i\frac{\hat{\sigma}_{nm}}{\omega}$ is usually called complex permittivity. By means of the constrains (2) and (4) the system of Equation (6) can be expressed in terms of electric field components only. Moreover, it can be reduced to only two equations, for example in terms of components E_1 and E_2. For this purpose we determined component E_3 from the third equation ($n = 3$) in (6):

$$E_3(z) = -i\frac{dE_1(z)}{dz}\frac{C_2}{C_1} - i\frac{dE_2(z)}{dz}\frac{C_3}{C_1} - E_1(z)\frac{C_4}{C_1} - E_2(z)\frac{C_5}{C_1}, \tag{7}$$

and substituted $E_3(z)$ into the equations given for $n = 1$, 2. After some straightforward algebra, the system of Equation (6) can be transformed into a SLME for the unknowns E_1 and E_2:

$$\frac{d}{dz}\left[B_{\gamma\eta}\frac{dE_\eta(z)}{dz} + P_{\gamma\eta}E_\eta(z)\right] + Y_{\gamma\eta}\frac{dE_\eta(z)}{dz} + W_{\gamma\eta}E_\eta(z) = 0; \quad \gamma,\eta = 1,2, \tag{8}$$

with matrix coefficients:

$$\mathbf{B}(z) = \begin{bmatrix} \left(\frac{C_2^2}{C_1} - \hat{\nu}_{22}\right) & \left(\frac{C_2C_3}{C_1} + \hat{\nu}_{12}\right) \\ \left(\frac{C_2C_3}{C_1} + \hat{\nu}_{12}\right) & \left(\frac{C_3^2}{C_1} - \hat{\nu}_{11}\right) \end{bmatrix}; \tag{9}$$

$$\mathbf{P}(z) = \begin{bmatrix} i\left(\hat{\nu}_{23}\kappa_2 - \frac{C_2C_4}{C_1}\right) & -i\left(\hat{\nu}_{23}\kappa_1 + \frac{C_2C_5}{C_1}\right) \\ -i\left(\hat{\nu}_{13}\kappa_2 + \frac{C_3C_4}{C_1}\right) & i\left(\hat{\nu}_{13}\kappa_1 - \frac{C_3C_5}{C_1}\right) \end{bmatrix}; \tag{10}$$

$$\mathbf{Y}(z) = \begin{bmatrix} i\left(\hat{\nu}_{23}\kappa_2 - \frac{C_2C_4}{C_1}\right) & -i\left(\hat{\nu}_{13}\kappa_2 + \frac{C_3C_4}{C_1}\right) \\ -i\left(\hat{\nu}_{23}\kappa_1 + \frac{C_2C_5}{C_1}\right) & i\left(\hat{\nu}_{13}\kappa_1 - \frac{C_3C_5}{C_1}\right) \end{bmatrix}; \tag{11}$$

$$\mathbf{W}(z) = \begin{bmatrix} \left(C_7 - \frac{C_4^2}{C_1}\right) & -\left(C_6 + \frac{C_5C_4}{C_1}\right) \\ -\left(C_6 + \frac{C_5C_4}{C_1}\right) & \left(C_8 - \frac{C_5^2}{C_1}\right) \end{bmatrix}. \tag{12}$$

The components of magnetic field $\overline{H}$ in terms of components E_1 and E_2 and the expressions for parameters from C_1 to C_9 are given in the Appendix A.

2.1. SLME Analysis

The SLME expressed in (8) has three important properties: 1) In the case of an homogeneous layer the linearly independent (LI) solutions of the differential equations system (8) can be expressed by means of exponentials [18, 19]:

$$\overline{E}_T(z) = \begin{vmatrix} E_{01} \\ E_{02} \end{vmatrix} e^{ikz}, \tag{13}$$

and we obtain the following Quadratic Eigenvalues Problem (QEP) [3]:

$$\left(-k^2\mathbf{B} + ik(\mathbf{P}+\mathbf{Y}) + \mathbf{W}\right) \cdot \begin{vmatrix} E_{01} \\ E_{02} \end{vmatrix} = \mathbf{0}_{2\times 1}, \tag{14}$$

whose solutions result in the eigenvalues k_ℓ and the eigenfunctions $\overline{E}_{T\ell}(z)$. If matrix $\mathbf{B}$ is *regular* ($\mathrm{Det}[\mathbf{B}] \neq 0$) we have a set of eigenvalues $K = \{k_\ell,\, \ell = 1, 2, 3, 4\}$ and the corresponding eigenfunctions:

$$\overline{E}_{T\ell}(z) = \left| \begin{array}{c} E_{01,\ell} \\ E_{02,\ell} \end{array} \right| e^{ik_\ell z}. \tag{15}$$

Finally the transverse electric field $\overline{E}_T(z)$, solution of Equation (8) for an homogeneous layer, can be expressed by means of a linear combination:

$$\overline{E}_T(z) = \left| \begin{array}{c} E_1(z) \\ E_2(z) \end{array} \right| = \sum_{\ell=1}^{4} a_\ell \overline{E}_{T\ell}(z), \tag{16}$$

where a_1, a_2, a_3, a_4 is a set of expansion coefficients.

Assuming a heterostructure consisting of homogeneous constituent layers, where the matrix coefficients $\mathbf{B}(z)$, $\mathbf{P}(z)$, $\mathbf{Y}(z)$, and $\mathbf{W}(z)$ do depend on z but are piecewise constants, we can obtain a 4×4 layer transfer matrix by means of the algebraic algorithms described in [1]:

$$\mathbf{T}(z, z_0) = \left| \begin{array}{cccc} \overline{E}_{T1}(z) & \overline{E}_{T2}(z) & \overline{E}_{T3}(z) & \overline{E}_{T4}(z) \\ \overline{A}_1(z) & \overline{A}_2(z) & \overline{A}_3(z) & \overline{A}_4(z) \end{array} \right| \cdot \left| \begin{array}{cccc} \overline{E}_{T1}(z_0) & \overline{E}_{T2}(z_0) & \overline{E}_{T3}(z_0) & \overline{E}_{T4}(z_0) \\ \overline{A}_1(z_0) & \overline{A}_2(z_0) & \overline{A}_3(z_0) & \overline{A}_4(z_0) \end{array} \right|^{-1}, \tag{17}$$

where $\overline{A}_\ell(z) = \mathbf{B} \cdot \frac{d\overline{E}_{T\ell}(z)}{dz} + \mathbf{P} \cdot \overline{E}_{T\ell}(z)$ is the linear form associated to the differential operator $\mathbf{L}(z)$ corresponding to the eigenfunction $\overline{E}_{T\ell}(z)$. This matrix transfers the transverse electric field $\overline{E}_T(z)$ and the corresponding linear form $\overline{A}(z)$ from z_0 to z inside a layer:

$$\left| \begin{array}{c} \overline{E}_T(z) \\ \overline{A}(z) \end{array} \right| = \mathbf{T}(z, z_0) \cdot \left| \begin{array}{c} \overline{E}_T(z_0) \\ \overline{A}(z_0) \end{array} \right|. \tag{18}$$

2) The linear form associated to the differential operator $\mathbf{L}(z)$ is continuous for every z along the multilayer structure [1]. In (8) the linear differential form is expressed as:

$$A_\gamma(z) = B_{\gamma\eta} \frac{dE_\eta(z)}{dz} + P_{\gamma\eta} E_\eta(z); \quad \gamma, \eta = 1, 2, \tag{19}$$

and its calculations leads to $A_1(z) = -i\omega H_2(z)$ and $A_2(z) = i\omega H_1(z)$ which means continuity of tangential components of the magnetic field. Besides this, continuity of $E_\eta(z)$ and $A_\eta(z)$ yields directly the well known chain property of matrix $\mathbf{T}$ [1].

3) Formal hemiticity of Sturm-Liouville differential operator requires $\mathbf{B} = \mathbf{B}^\dagger$, $\mathbf{W} = \mathbf{W}^\dagger$ and $\mathbf{Y} = -\mathbf{P}^\dagger$ [1], the symbol $\dagger$ means Hermitean conjugate operation. Accordingly, the eigenvalues of the QEP satisfy the general property of being real or appearing in pairs: k_ℓ and its complex conjugate k_ℓ^*.

The determinant of matrix $\mathbf{T}$ can be expressed using the equation [1]:

$$\mathrm{Det}[\mathbf{T}(z, z_0)] = e^{\int_{z_0}^{z} dz \mathrm{Tr}[\mathbf{D}(z)]}; \quad \mathrm{Tr}[\mathbf{D}(z)] = -\mathrm{Tr}\left[\mathbf{B}(z)^{-1} \cdot \{\mathbf{P}(z) + \mathbf{Y}(z)\}\right], \tag{20}$$

where $\mathrm{Tr}[\mathbf{D}(z)]$ means trace of matrix $\mathbf{D}(z)$. If the hermiticity condition holds, then $\mathrm{Tr}[\mathbf{D}(z)]$ becomes imaginary [1] and we can write: $\mathrm{Det}[\mathbf{T}(z, z_0)] = e^{i\Theta(z)}$ where $\Theta(z)$ is real and consequently the determinant of matrix $\mathbf{T}$ is unimodular: $|\mathrm{Det}[\mathbf{T}]| = 1$. Moreover, if $\mathrm{Tr}[\mathbf{D}(z)] = 0$ then $\mathrm{Det}[\mathbf{T}] = 1$. This outcome can be used in practice to keep a check on the numerical quality of a calculation as $|z - z_0|$ grows. For complex eigenvalues we have from (15) and (17) that matrix $\mathbf{T}$ elements shall have combinations of decreasing and increasing exponentials, and for example, if $|z - z_0|$ grows the difference in order of magnitude between the largest and the smallest number may exceeds the computer accuracy and it results in a numerical degradation. In this cases the value of $\mathrm{Det}[\mathbf{T}]$ deviates from unity by more than the accepted limit.

Moreover as the stack transfer matrix is obtained by multiplication of the matrices corresponding to each layer of the heterostructure (the chain property of matrix $\mathbf{T}$), even if none of the constituent layers is sufficiently large to cause an Ωd problem by itself, numerical degradation may accumulate due to a large number of matrices involved in calculation [1]. This means that calculations should be monitored to be sure that numerical accuracy is under control. For example, if the hermiticity condition holds, the determinant of the stack transfer matrix should also be unimodular and it can be used for this purpose.

For anisotropic media with $\hat{\sigma} = \mathbf{0}$ parameters C_1, C_4, C_5, C_6, C_7 and C_8 (see A.2) become real assuming that $\hat{\epsilon}$ and $\hat{\mu}$ are real tensors. Then the analysis of matrices given by (9)–(12) indicates that formal hermiticity condition holds, and therefore $|\mathrm{Det}[\mathbf{T}]| = 1$. In this case eigenvalues satisfy the general property of being real or appearing in pairs: (k_ℓ, k_ℓ^*) as mentioned above. On the other hand, if $\hat{\sigma} \neq \mathbf{0}$ then hermiticity condition doesn't holds and usually $\mathrm{Det}[\mathbf{T}] \neq 1$. In this case we must expect wave attenuation in z direction due to electric conductivity of medium, which means that k_ℓ must be complex according to expression (15). In both cases $\hat{\sigma} \neq \mathbf{0}$ and $\hat{\sigma} = \mathbf{0}$ the same transfer matrix techniques (17) applies and we can deal with complex eigenvalues, so that numerical accuracy must be monitored.

3. ELECTROMAGNETIC-WAVE PROPAGATION IN LINEAR LAYERED ISOTROPIC MEDIA

We applied analysis given in Section 2 to wave propagation in linear layered isotropic media. In this case tensors $\hat{\epsilon} = \epsilon(z)\mathbf{I}$, $\hat{\nu} = \frac{1}{\mu(z)}\mathbf{I}$ and $\hat{\sigma} = \sigma(z)\mathbf{I}$ with $\mathbf{I}$ denoting the 3×3 identity matrix. The wave vector $\overline{\kappa} = (\kappa_1, \kappa_2)$ can be chosen as $\overline{\kappa} = (0, \kappa)$. Under this conditions, equations involved in (8) decouple and result:

$$\frac{d}{dz}\left[\frac{1}{\mu(z)}\frac{dE_1(z)}{dz}\right] + E_1(z)\left[\omega^2\tilde{\epsilon}(z) - \frac{\kappa^2}{\mu(z)}\right] = 0; \tag{21}$$

$$\frac{d}{dz}\left[\left(\frac{\omega^2\tilde{\epsilon}(z)}{\kappa^2 - \omega^2\tilde{\epsilon}(z)\mu(z)}\right)\frac{dE_2(z)}{dz}\right] - \omega^2\tilde{\epsilon}(z)E_2 = 0, \tag{22}$$

where $\tilde{\epsilon}(z) = \epsilon(z) + i\frac{\sigma(z)}{\omega}$. In both equations continuity of tangential components of magnetic fields is implicit, due to continuity of the linear differential form.

Equations (21) and (22) can be treated as two independent SLME, then a 2×2 transfer matrix $\mathbf{T}$ can be obtained from each one. For both equations hermiticity condition doesn't holds, but $\mathbf{P} = \mathbf{Y} = 0$; therefore, $\mathbf{D}(z) = 0$ and $\mathrm{Det}[\mathbf{T}] = 1$. For clarity let's focus on equation for component E_1 (for component E_2 the procedure is the same). For an homogeneous slab, eigenvalues $k_1 = +k$, $k_2 = -k$; $k = \sqrt{\omega^2\tilde{\epsilon}\mu - \kappa^2}$ and LI solutions : e^{ikz}, e^{-ikz} ($E_{01,1} = 1$; $E_{01,2} = 1$) leads to:

$$E_1(z) = a_1 e^{ikz} + a_2 e^{-ikz}. \tag{23}$$

In this case eigenvalues $\pm k$ are complex due to complex permittivity $\tilde{\epsilon}$. We can write k as the sum of a real and a imaginary part: $k = k_R + ik_I$ and the wave given in (23) will be characterized by attenuation of its amplitude in z direction. For the conducting medium, wave attenuation in the direction of propagation can be obtained using Maxwell's equations in charge-free regions [20].

Using (17) with $\overline{E}_{T3}(z/z_0) = 0$, $\overline{A}_3(z/z_0) = 0$ and $\overline{E}_{T4}(z/z_0) = 0$, $\overline{A}_4(z/z_0) = 0$, we obtain:

$$\mathbf{T}(z, z_0) = \begin{pmatrix} \cos k(z - z_0) & \frac{\mu}{k}\sin k(z - z_0) \\ -\frac{k}{\mu}\sin k(z - z_0) & \cos k(z - z_0) \end{pmatrix}, \tag{24}$$

and from (18):

$$\begin{vmatrix} E_1(z) \\ i\omega H_2(z) \end{vmatrix} = \mathbf{T}(z, z_0) \cdot \begin{vmatrix} E_1(z_0) \\ i\omega H_2(z_0) \end{vmatrix}. \tag{25}$$

Since k is complex, matrix elements of $\mathbf{T}(z, z_0)$ in fact contain algebraic sums of real exponentials: $e^{|k_I|d}$ and $e^{-|k_I|d}$, where $d = z - z_0$; the argument $|k_I|\, d$ increase when thickness d and/or frequency ω increases. As mentioned above, the mixture of growing and decaying terms may leads to inaccuracy during computations, a process we can monitor through the theoretical result $\mathrm{Det}[\mathbf{T}] = 1$. Moreover, when $k_I d \to \infty$ elements of matrix (24) become infinity due to growing exponential $e^{|k_I|d}$.

The Hybrid Compliance-Stiffnes matrix was employed in [15] as a stable variant to study the propagation of an acoustic wave in an anisotropic multilayer system. This matrix, denoted here by $\mathbf{Hy}$ can be defined by changing the arrangement of the $\overline{E}_T(z)$, $\overline{A}(z)$, $\overline{E}_T(z_0)$ and $\overline{A}(z_0)$ vectors in (18):

$$\begin{vmatrix} \overline{E}_T(z_0) \\ \overline{A}(z) \end{vmatrix} = \mathbf{Hy}(z; z_0) \cdot \begin{vmatrix} \overline{A}(z_0) \\ \overline{E}_T(z) \end{vmatrix}. \tag{26}$$

The hybrid compliance-stiffness matrix, or simply hybrid matrix, **Hy** can be obtained by means of its relation [15] with partitions of **T**, so in this case we have:

$$\mathbf{Hy}(z,z_0)=\begin{pmatrix} -\frac{\mu}{k}\tan k(z-z_0) & \frac{1}{\cos k(z-z_0)} \\ \frac{1}{\cos k(z-z_0)} & -\frac{k}{\mu}\tan k(z-z_0) \end{pmatrix}, \tag{27}$$

and

$$\begin{vmatrix} E_1(z_0) \\ i\omega H_2(z) \end{vmatrix} = \mathbf{Hy}(z,z_0)\cdot \begin{vmatrix} i\omega H_2(z_0) \\ E_1(z) \end{vmatrix}. \tag{28}$$

In hybrid matrix only decreasing exponentials terms are involved and because of that it is numerically stable [15]. For complex eigenvalues, matrix elements of **Hy** in fact may be expressed in terms of decreasing exponentials $e^{-|k_I|d}$ and bounded terms only. Moreover, when $k_I d \to \infty$ **Hy** reduces to:

$$\mathbf{Hy}|_{(k_I d)\to\infty}=\begin{pmatrix} -\frac{\mu}{k} & 0 \\ 0 & -\frac{k}{\mu} \end{pmatrix}. \tag{29}$$

The hybrid matrix for the entire heterostructure (the stack hybrid matrix) can be determined by the recursive algorithm given in [15].

3.1. Transverse Electric (TE) and Transverse Magnetic (TM) Waves

For isotropic media the component E_3 of electric field, obtained from Equation (7), is:

$$E_3(z)=-i\left(\frac{\kappa}{\kappa^2-\omega^2\tilde{\epsilon}(z)\mu(z)}\right)\frac{dE_2(z)}{dz}, \tag{30}$$

and the components of magnetic field, obtained from expressions given in the Appendix A, are:

$$H_1(z) = -\frac{i}{\omega}\left(\frac{\omega^2\tilde{\epsilon}(z)}{\kappa^2-\omega^2\tilde{\epsilon}(z)\mu(z)}\right)\frac{dE_2(z)}{dz}; \tag{31}$$

$$H_2(z) = -\frac{i}{\mu(z)\omega}\frac{dE_1(z)}{dz}; \tag{32}$$

$$H_3(z) = -\frac{\kappa E_1(z)}{\omega\mu(z)}. \tag{33}$$

Transverse electric wave means $E_3 = 0$, then from (30)–(31) we have component $H_1 = 0$ and from (22) that $E_2 = 0$. On the other hand, if $E_1 \neq 0$ then from (33) and (32) we have that magnetic field keeps its components H_3 and H_2. The component E_1 is calculated from (21).

Transverse magnetic wave means $H_3 = 0$, then from (33) we obtain $E_1 = 0$ and consequently from (32) we have $H_2 = 0$. Besides, if $H_1 \neq 0$ then from (31), (30) and (22) we have that electric field keeps its components E_3 and E_2. Combining (22) with (31) we obtained:

$$\frac{d}{dz}\left[\frac{1}{\tilde{\epsilon}(z)}\frac{dH_1(z)}{dz}\right]+H_1(z)\left(\mu(z)\omega^2-\frac{\kappa^2}{\tilde{\epsilon}(z)}\right)=0. \tag{34}$$

If condition $E_3 = 0$ and $H_3 = 0$ is imposed, then from Eqs. (30)–(33) and (22) follows immediately that all components of electric and magnetic field vanishes. This means, as expected, that in the analyzed case transverse electromagnetic wave doesn't exist.

Taking into account that $E_m = E_m(z)e^{i(\kappa y-\omega t)}$, $H_m = H_m(z)e^{i(\kappa y-\omega t)}$; $\vec{\kappa}=(0,\kappa)$ and considering an homogenous nonconducting medium we can write the following expressions:

$$H_3 = -\frac{1}{i\omega\mu}\frac{\partial E_1}{\partial y}; \quad \text{from (33)}, \tag{35}$$

$$H_2 = \frac{1}{i\omega\mu}\frac{\partial E_1}{\partial z}; \quad \text{from (32)}, \tag{36}$$

$$\left(\frac{\partial^2}{\partial z^2}+\frac{\partial^2}{\partial y^2}+\omega^2\mu\epsilon\right)E_1=0;\quad \text{from (21)}, \tag{37}$$

$$E_2=-\frac{1}{i\omega\epsilon}\frac{\partial H_1}{\partial z};\quad \text{from (22) and (31)}, \tag{38}$$

$$E_3=\frac{1}{i\omega\epsilon}\frac{\partial H_1}{\partial y};\quad \text{from (30) and (31)}, \tag{39}$$

$$\left(\frac{\partial^2}{\partial z^2}+\frac{\partial^2}{\partial y^2}+\omega^2\mu\epsilon\right)H_1=0;\quad \text{from (34)}. \tag{40}$$

Then renaming z axis as x and y axis as z and considering that now subindexes 1, 2, 3 represent axis y, z, x respectively, we obtain the equations (4.1.58 to 4.1.63) given in [20] for TE and TM waves.

4. NUMERICAL EXAMPLES

4.1. The Anisotropic Layered System

A Fabry-Perot microcavity structure [21] was analyzed as a simple example of anisotropic layered system. The layers material of this structure consist of anisotropic mesoporous silicon exhibiting optical birefringence given by an artificial in-plane uniaxial symmetry [22]. The analyzed Fabry-Perot microcavity structure is made up of two Bragg mirrors (each formed by 12 pairs of alternating mesoporous silicon layers with two different refractive indices and an optical thickness equal to $\lambda_0/4$) separated by a microcavity layer with an optical thickness equal to $\lambda_0/2$. λ_0 is the central wavelength of Bragg mirror radiation spectrum. The ordinary n_0 and extraordinary n_e refractive indices of the alternating layers are $n_{01}=1.39$, $n_{02}=1.58$ and $n_{e1}=1.32$, $n_{e2}=1.50$. According to [21] the wavelength $\lambda_0=850\,\text{nm}$ and the anisotropy of the refractive indices was found at wavelength $\lambda=800\,\text{nm}$.

In this case we can chose the optic axis to be in the z direction. Then each of layers is characterized by a permittivity tensor $\hat{\epsilon}$:

$$\tilde{\epsilon}=\frac{1}{c^2}\begin{pmatrix}(n_0+i\xi_0)^2 & 0 & 0\\ 0 & (n_0+i\xi_0)^2 & 0\\ 0 & 0 & (n_e+i\xi_e)^2\end{pmatrix}, \tag{41}$$

where ξ denotes the extinction coefficient and c the speed of light in vacuum; permeability $\mu=1$ was considered. It is considered that the incident EM wave is coming from the air, then the wave vector components are:

$$\kappa_x = \frac{\omega}{c}n_a\sin\theta\sin\varphi \tag{42}$$

$$\kappa_y = \frac{\omega}{c}n_a\sin\theta\cos\varphi, \tag{43}$$

where n_a is the refractive index of air. The angle of incidence θ is measured from the z axis and the azimuthal angle φ from the y axis. Consider $\varphi=0^\circ$ then component E_1 corresponds to the s-polarized wave and E_2 to the p-polarized wave. Under this condition and using (41) the equations involved in (8) decouple and result:

$$\frac{d^2E_1(z)}{dz^2}+\frac{\omega^2}{c^2}\left[(n_0+i\xi_0)^2-(n_a\sin\theta)^2\right]E_1(z) = 0; \tag{44}$$

$$\frac{d^2E_2(z)}{dz^2}+\frac{\omega^2}{c^2}\frac{(n_0+i\xi_0)^2}{(n_e+i\xi_e)^2}\left[(n_e+i\xi_e)^2-(n_a\sin\theta)^2\right]E_2(z) = 0. \tag{45}$$

For both equations eigenvalues are $\pm k$; $k=\frac{\omega}{c}\sqrt{(n_0+i\xi_0)^2-(n_a\sin\theta)^2}$ for Equation (44) and $k=\frac{\omega}{c}\left(\frac{n_0+i\xi_0}{n_e+i\xi_e}\right)\sqrt{(n_e+i\xi_e)^2-(n_a\sin\theta)^2}$ for Equation (45). Therefore in this case both components $E_1(z)$ and $E_2(z)$ can be calculated using a 2×2 associated transfer matrix as in the isotropic case.

The reflection coefficient (r) was calculated for components E_1 and E_2 at an angle of incidence $\theta = 20°$ for the azimuthal angle $\varphi = 0°$ using expressions given in Appendix B in terms of the stack matrix $\mathbf{T}_h$. In our calculus we consider constant both the refractive index and the extinction coefficient in the analyzed wavelength range, and to simplify the calculus we assume the single value $\xi_0 = \xi_e = 0.004$. The $|r|^2$ dependence with wavelength for s- and p-polarized waves is given in Figure 1. The spectra show a microcavity mode for both polarizations. For s-polarized wave we obtained a microcavity mode at wavelength $\lambda_{mc} = 827$ nm in good agreement with the corresponding experimental spectrum shown in [21] for which $\lambda_{mc} = 830$ nm. As in the experimental spectra a change in λ_{mc} position is observed when the polarization of the incident light is switched. With p-polarized wave at an angle of incidence $\theta = 25°$ the shift of the microcavity mode was calculated around to 17 nm. For the analyzed wavelength range $\mathrm{Det}[\mathbf{T}_h] = 1$ as was predicted analytically for $\mathbf{P} = \mathbf{Y} = \mathbf{0}$.

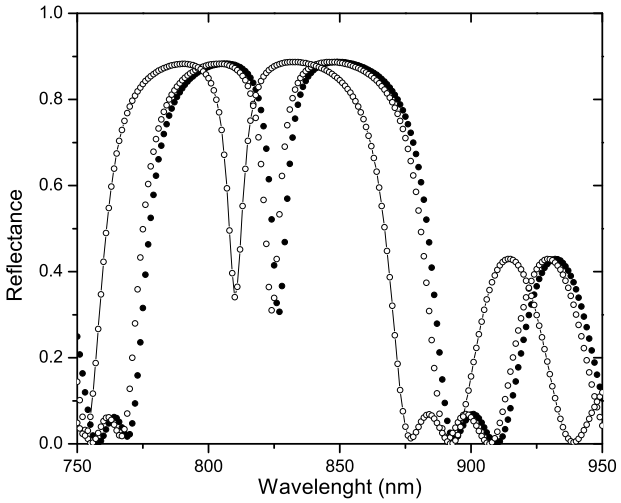

Figure 1. Reflectance spectra of a microcavity structure calculated with electric components E_1 (filled circles) and E_2 (open circles) at an angle of incidence $\theta = 20°$ and calculated with component E_2 at an angle of incidence $\theta = 25°$ (line + open circles). The azimuthal angle $\varphi = 0°$.

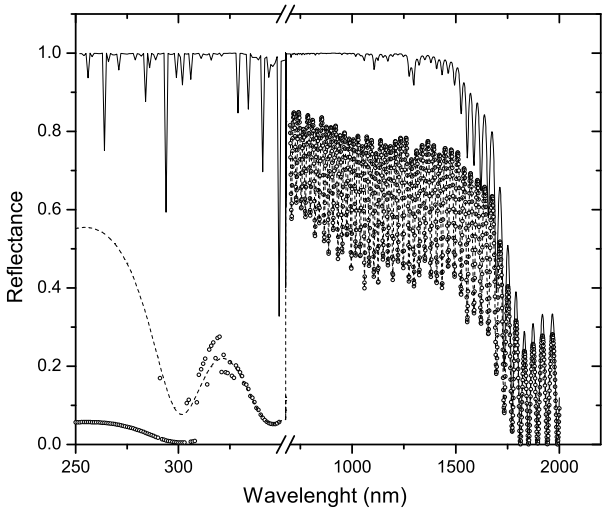

Figure 2. Reflectance spectrum of a PSPM calculated for the two cases: 1) considering negligible the porous silicon absorption and using stack matrix $\mathbf{T}_h$ (solid line); and 2) considering porous silicon absorption, using stack matrix $\mathbf{Hy_h}$ (dashed line) and using stack matrix $\mathbf{T}_h$ (open circles).

4.2. The Isotropic Layered System

A porous silicon photonic mirror (PSPM) is used here as an example of layered isotropic system. The PSPMs are multilayers of two alternated refractive indices where the condition $\lambda_0/4$ in the optical path is imposed. Our model structure is composed of 20 submirrors and is based on PSPM structures analyzed in [23]. Our submirrors consist in ten alternating porous silicon layers with refractive indices $n_{01} = 1.5$ and $n_{02} = 2.0$. We selected to reflect the wavelength range from 250 nm to 1500 nm. From the 1th submirror ($\lambda_{01} = 250$ nm) to the 16th submirror ($\lambda_{016} = 1000$ nm) the central wavelength increase in 50 nm. From the 17th submirror ($\lambda_{017} = 1100$ nm) to the 20th submirror ($\lambda_{020} = 1500$ nm) the central wavelength increase in 100 nm.

For normal incidence, eigenvalues are $\pm k$; $k = \frac{\omega}{c}(n_0 + i\xi)$; $\mu = 1$. Using expressions given in Appendix B the reflection coefficient r was calculated (for $\theta = 0$) in terms of the stack transfer matrix $\mathbf{T}_h$ considering negligible the porous silicon absorption. As expected we obtained high reflectance from 250 nm to 1500 nm, see Figure 2. On the other hand to simulate the strong absorption of porous silicon in the wavelengths region 250–413 nm a constant extinction coefficient value $\xi = 0.08$ was set. For longer wavelengths a smaller extinction coefficient value $\xi = 0.0013$ was considered. These only two values of ξ were considered in order to simplify the calculation and were estimated from a measured

absorption coefficient spectra [24].

In order to analyze the numerical stability of transfer matrix in presence of strong absorption we calculated the reflection coefficient in terms of stack matrices $\mathbf{T}_h$ and $\mathbf{Hy_h}$ for $\theta = 0$. In the wavelengths range 250–300 nm we obtained $10^{18} \leq |\mathrm{Det}[\mathbf{T}_h]| \leq 10^{23}$ and $|\mathrm{Det}[\mathbf{Hy_h}]| \leq 1$ and reflectance values calculated with matrix $\mathbf{T}_h$ differ significantly from those calculated with $\mathbf{Hy_h}$, as shown in Figure 2. However, longer wavelengths do not suffer significant losses and both reflectance spectra coincide. As would be expected the reflectance is reduced in the presence of absorption.

In this particular problem we can obtain the same accurate result that we obtained with $\mathbf{Hy_h}$ despite the numerical instability of $\mathbf{T}_h$ using a different expression to calculate the reflection coefficient, for example:

$$r = -\frac{n_c T_{h11} + n_a n_c T_{h12} - T_{h21} - n_a T_{h22}}{n_c T_{h11} - n_a n_c T_{h12} - T_{h21} + n_a T_{h22}}, \tag{46}$$

where n_a/n_c is the refractive index of air/crystalline silicon, see Appendix B. In this case numerical instability of $\mathbf{T}_h$ continues affecting the accuracy of the matrix elements T_{h11}, T_{h12}, T_{h21} and T_{h22}, but in this case the ratio of the two quantities leads to a very accurate result due to cancellation of rounding errors [17]. Probably this is the reason why the numerical instability of the 2×2 stack transfer matrix is not perceived in problems involving layered isotropic media.

5. CONCLUSION

In summary, we have established an Sturm-Lioville matrix equation of motion for the study of electromagnetic wave propagation in linear anisotropic layered structures in terms of tangential components of electric field. This equation involve ohmic losses and is suitable to develop 4×4 associated transfer matrix methods in heterostructure where the tensors: permittivity, permeability and the electric conductivity have a piecewise dependence on the coordinate perpendicular to the layered structure.

For layered anisotropic media we have shown analytically that when conductivity tensor is null, Sturm-Liouville differential operator is formally hermitian and consequently the determinant of the associate transfer matrix is unimodular. In this case Ωd problem, which is more likely for complex eigenvalues, can be monitored through the resulting numerical value of $|\mathrm{Det}[\mathbf{T}]|$. For the conducting medium, we also expect obtain complex eigenvalues and the numerical quality of calculations should also be monitored but considering that $\mathbf{T}$ determinant could be different from 1.

For layered isotropic media it was determined that $\mathrm{Det}[\mathbf{T}] = 1$. In this case a more simple 2×2 associated transfer matrix was obtained. For the conducting isotropic medium we have found that Ωd problem may arise at high frequencies and/or big thickness of the layers. Using relation between matrices a 2×2 hybrid matrix was obtained from $\mathbf{T}$ and it was found that it can avoid the numerical degradation as well as in elasticity-theory problems. Expressions for TE and EM waves were reproduced.

The reflectance spectrum for a Fabry-Perot microcavity structure whose layers consist of mesoporous silicon exhibiting optical birefringence was calculated using a 2×2 transfer matrix. In this layered anisotropic structure, porous silicon absorption was considered and the good agreement with experimental measures confirms that the SLME approach can be used to analyze EM wave propagation in layered anisotropic structure in a straightforward way. The reflectance spectrum for a porous silicon photonic mirror (layered isotropic system) was calculated in terms of both the transfer matrix and the hybrid matrix and numerical instability of transfer matrix was verified at high frequencies (low wavelengths) in presence of strong porous silicon absorption. We showed that even when the 2×2 transfer matrix is affected by numerical instability it is possible to obtain accurate reflection coefficient values due to the cancellation of rounding errors .

ACKNOWLEDGMENT

R. P.-S. acknowledges CONACyT support. R. P.-A. also acknowledges CONACyT support through grant 208108.

APPENDIX A. EXPRESSIONS FOR COMPONENTS OF MAGNETIC FIELD AND PARAMETER C

A.1. Components of Magnetic Field in Terms of Electric Components E_1 and E_2

$$\begin{aligned} H_1(z) &= -\frac{dE_1(z)}{dz}\frac{i}{\omega}\left(\hat{\nu}_{12}+\frac{C_2C_3}{C_1}\right)+\frac{dE_2(z)}{dz}\frac{i}{\omega}\left(\hat{\nu}_{11}-\frac{C_3^2}{C_1}\right) \\ &\quad -\frac{E_1(z)}{\omega}\left(\kappa_2\hat{\nu}_{13}+\frac{C_4C_3}{C_1}\right)+\frac{E_2(z)}{\omega}\left(\kappa_1\hat{\nu}_{13}-\frac{C_5C_3}{C_1}\right); \qquad \text{(A1)} \\ H_2(z) &= \frac{dE_1(z)}{dz}\frac{i}{\omega}\left(\frac{C_2^2}{C_1}-\hat{\nu}_{22}\right)+\frac{dE_2(z)}{dz}\frac{i}{\omega}\left(\hat{\nu}_{12}+\frac{C_2C_3}{C_1}\right) \\ &\quad +\frac{E_1(z)}{\omega}\left(\frac{C_4C_2}{C_1}-\kappa_2\hat{\nu}_{23}\right)+\frac{E_2(z)}{\omega}\left(\frac{C_5C_2}{C_1}+\kappa_1\hat{\nu}_{23}\right); \qquad \text{(A2)} \\ & \qquad \text{(A3)} \\ H_3(z) &= -\frac{dE_1(z)}{dz}\frac{i}{\omega}\left(\hat{\nu}_{23}+\frac{C_2C_9}{C_1}\right)+\frac{dE_2(z)}{dz}\frac{i}{\omega}\left(\hat{\nu}_{13}-\frac{C_3C_9}{C_1}\right) \\ &\quad -\frac{E_1(z)}{\omega}\left(\kappa_2\hat{\nu}_{33}+\frac{C_4C_9}{C_1}\right)+\frac{E_2(z)}{\omega}\left(\kappa_1\hat{\nu}_{33}-\frac{C_5C_9}{C_1}\right). \qquad \text{(A4)} \end{aligned}$$

A.2. Parameters C_1 to C_9

$$\begin{aligned} C_1 &= \kappa_2^2\hat{\nu}_{11}-2\kappa_1\kappa_2\hat{\nu}_{12}+\kappa_1^2\hat{\nu}_{22}-\omega^2\left(\hat{\epsilon}_{33}+i\frac{\hat{\sigma}_{33}}{\omega}\right); \qquad \text{(A5)} \\ C_2 &= \kappa_1\hat{\nu}_{22}-\kappa_2\hat{\nu}_{12}; \qquad \text{(A6)} \\ C_3 &= \kappa_2\hat{\nu}_{11}-\kappa_1\hat{\nu}_{12}; \qquad \text{(A7)} \\ C_4 &= \kappa_1\kappa_2\hat{\nu}_{23}-\kappa_2^2\hat{\nu}_{13}-\omega^2\left(\hat{\epsilon}_{13}+i\frac{\hat{\sigma}_{13}}{\omega}\right); \qquad \text{(A8)} \\ C_5 &= \kappa_1\kappa_2\hat{\nu}_{13}-\kappa_1^2\hat{\nu}_{23}-\omega^2\left(\hat{\epsilon}_{23}+i\frac{\hat{\sigma}_{23}}{\omega}\right); \qquad \text{(A9)} \\ C_6 &= \kappa_1\kappa_2\hat{\nu}_{33}+\omega^2\left(\hat{\epsilon}_{12}+i\frac{\hat{\sigma}_{12}}{\omega}\right); \qquad \text{(A10)} \\ C_7 &= \kappa_2^2\hat{\nu}_{33}-\omega^2\left(\hat{\epsilon}_{11}+i\frac{\hat{\sigma}_{11}}{\omega}\right); \qquad \text{(A11)} \\ C_8 &= \kappa_1^2\hat{\nu}_{33}-\omega^2\left(\hat{\epsilon}_{22}+i\frac{\hat{\sigma}_{22}}{\omega}\right); \qquad \text{(A12)} \\ C_9 &= \kappa_2\hat{\nu}_{13}-\kappa_1\hat{\nu}_{23}. \qquad \text{(A13)} \end{aligned}$$

APPENDIX B. CALCULATION OF THE REFLECTION AND TRANSMISSION COEFFICIENTS

The layered systems analyzed in Section 4 were bounded between air and a crystalline silicon (c-Si) substrate. Considering the incident, reflected and transmitted amplitudes of the electric component E_1 (or E_2) the reflection (r) and the transmission (t) coefficients, for both systems, can be expressed in

terms of its stack matrices $\mathbf{T}_h$ or $\mathbf{Hy}_h$:

$$\begin{pmatrix} r \\ t \end{pmatrix} = \left[\begin{pmatrix} 0 & 1 \\ 0 & \sqrt{n_c^2 - (n_a \sin\theta)^2} \end{pmatrix} - \mathbf{T}_h \cdot \begin{pmatrix} 1 & 0 \\ -n_a \cos\theta & 0 \end{pmatrix} \right]^{-1} \cdot \mathbf{T}_h \cdot \begin{pmatrix} 1 \\ n_a \cos\theta \end{pmatrix}; \tag{B1}$$

$$\begin{pmatrix} r \\ t \end{pmatrix} = \left[\begin{pmatrix} 1 & 0 \\ 0 & \sqrt{n_c^2 - (n_a \sin\theta)^2} \end{pmatrix} - \mathbf{Hy}_h \cdot \begin{pmatrix} -n_a \cos\theta & 0 \\ 0 & 1 \end{pmatrix} \right]^{-1} \cdot \left[\mathbf{Hy}_h \cdot \begin{pmatrix} n_a \cos\theta \\ 0 \end{pmatrix} - \begin{pmatrix} 1 \\ 0 \end{pmatrix} \right], \tag{B2}$$

where n_a/n_c is the refractive index of air/c-Si and θ is the angle of incidence. Matrices $\mathbf{T}_h$ and $\mathbf{Hy}_h$ were obtained by means of the corresponding recursive algorithm and using the layer matrix:

$$\mathbf{T}(d) = \begin{pmatrix} \cos kd & i\frac{1}{f(k)} \sin kd \\ if(k) \sin kd & \cos kd \end{pmatrix}; \tag{B3}$$

and

$$\mathbf{Hy}(d) = \begin{pmatrix} -i\frac{1}{f(k)} \tan kd & \frac{1}{\cos kd} \\ \frac{1}{\cos kd} & if(k) \tan kd \end{pmatrix}, \tag{B4}$$

respectively, where $f(k) = (c/\omega)k$, layer thickness $d = \frac{\lambda_0}{4n_0}$ for Bragg mirror layers and $d = \frac{\lambda_0}{2n_0}$ for the microcavity layer; λ_0 is the central wavelength of the Bragg mirror radiation spectrum and n_0 is the refractive index for the isotropic layers and the ordinary refractive index for the anisotropic layers. Reflectance is given by $|r|^2$.

REFERENCES

1. Pérez-Álvarez, R. and F. García-Moliner, *Transfer Matrix, Green Function and Related Techniques: Tools for the Study of Multilayer Heterostructures*, Universitat Jaume I, Castellón de la Plana, Spain, 2004.
2. Trallero-Giner, C., R. Pérez-Alvarez, and F. García-Moliner, *Long Wave Polar Modes in Semiconductor Heterostructures*, Elsevier Science, Oxford GB, Pergamon, 1998.
3. Tisseur, F. and K. Meerbergen, "The quadratic eigenvalue problem," *SIAM Rev.*, Vol. 43, No. 2, 235–286, 2001.
4. Bonnet, G., "Orthotropic elastic media having a closed form expression of the Green tensor," *Int. J. Solids Struct.*, Vol. 46, No. 5, 1240–1250, 2009.
5. Li, X. and M. Wang, "Three-dimensional Green's functions for infinite anisotropic piezoelectric media," *Int. J. Solids Struct.*, Vol. 44, No. 5, 1680–1684, 2007.
6. Bastard, G. and J. A. Brum, "Electronic states in semiconductor heterostructures," *IEEE J. Quantum Elect.*, Vol. 22, No. 9, 1625–1644, 1986.
7. Bastard, G., *Wave Mechanics Applied to Semiconductor Heterostructures*, Éditions de Physique, Paris, 1989.
8. Oldano, C., "Electromagnetic-wave propagation in anisotropic stratified media," *Phys. Rev. A*, Vol. 40, No. 10, 6014–6020, 1989.
9. Berreman, D. W., "Optics in stratified and anisotropic media: 4×4-matrix formulation," *J. Opt. Soc. Am.*, Vol. 62, No. 4, 502–510, 1972.
10. Krijn, M. P. C. M., "Electromagnetic wave propagation in stratified anisotropic media in the presence of sources," *Opt. Lett.*, Vol. 17, No. 3, 163–165, 1992.
11. Jiaming, H. and Z. Lei, "Electromagnetic wave scatterings by anisotropic metamaterials: Generalized 4×4 transfer-matrix method," *Phys. Rev. B*, Vol. 77, No. 9, 094201-1–094201-12, 2008.
12. Calas, H., R. Rodriguez-Ramos, J. A. Otero, L. Leija, A. Ramos, and G. Monsivais, "Dispersion curves of shear horizontal wave surface velocities in multilayer piezoelectric systems," *J. Appl. Phys.*, Vol. 107, No. 4, 044511-1–044511-9, 2010.
13. Zhang, V. Y. and V. Laude, "Unified and stable scattering matrix formalism for acoustic waves in piezoelectric stacks," *J. Appl. Phys.*, Vol. 104, No. 6, 064916-1–064916-7, 2008.

14. Tan, E. L., "Matrix algorithms for modeling acoustic waves in piezoelectric multilayers," *IEEE Trans. Ultrason., Ferroelect., Freq. Contr.*, Vol. 54, No. 10, 2016–2023, 2007.
15. Tan, E. L., "Hybrid compliance-stiffness matrix method for stable analysis of elastic wave propagation in multilayered anisotropic media," *J. Acoust. Soc. Am.*, Vol. 119, No. 1, 45–53, 2006.
16. Lowe, M. J. S., "Matrix techniques for modeling ultrasonic waves in multilayered media," *IEEE Trans. Ultrason., Ferroelect., Freq. Contr.*, Vol. 42, No. 4, 525–542, 1995.
17. Higham, N. J., *Accuracy and Stability of Numerical Algorithms*, Society for Industrial and Applied Mathematics, Philadelphia, PA, USA, 2002.
18. Hurewicz, V., *Lectures on Ordinary Differential Equations*, The MIT Press, Cambridge, MA, 1958.
19. Bibikov, Y. N., *General Course on Ordinary Differential Equations (in Russian)*, Leningrad University Press, Leningrad, 1981.
20. Kong, J. A., *Electromagnetic Wave Theory*, EMW Publishing, Cambridge, Massachusetts, USA, 2008.
21. Aktsipetrov, O. A., T. V. Dolgova, I. V. Soboleva, and A. A. Fedyanin, "Anisotropic photonic crystals and microcavities based on mesoporous silicon," *Phys. Solid State*, Vol. 47, No. 1, 156–158, 2005.
22. Kovalev, D., G. Polisski, J. Diener, H. Heckler, N. Kunzner, V. Yu. Timoshenko, and F. Koch, "Strong in-plane birefringence of spatially nanostructured silicon," *Appl. Phys. Lett.*, Vol. 78, No. 7, 916–918, 2001.
23. De la Mora, M. B., O. A. Jaramillo, R. Nava, J. Tagüeña-Martínez, and J. A. del Río, "Viability study of porous silicon photonic mirrors as secondary reflectors for solar concentration systems," *Sol. Energy Mater. Sol. Cells*, Vol. 93, No. 8, 1218–1224, 2009.
24. Diesinger, H., A. Bsiesy, and R. Hérino, "In situ measurement of the optical absorption coefficient of porous silicon," *J. Appl. Phys.*, Vol. 89, No. 1, 221–225, 2001.